Molecular Simulation of the Interlayer Structure and the Mobility of Alkyl Chains in HDTMA + /Montmorillonite Hybrids

ARTICLE *in* THE JOURNAL OF PHYSICAL CHEMISTRY B · AUGUST 2005

Impact Factor: 3.3 · DOI: 10.1021/jp0517495 · Source: PubMed

3 AUTHORS, INCLUDING:

Hongping He
Chinese Academy of Sciences
191 PUBLICATIONS **4,590** CITATIONS
SEE PROFILE

Jean-François Gerard
Institut National des Sciences Appliquées de …
340 PUBLICATIONS **4,092** CITATIONS
SEE PROFILE

Molecular Simulation of the Interlayer Structure and the Mobility of Alkyl Chains in HDTMA$^+$/Montmorillonite Hybrids

Hongping He,*,†,‡ Jocelyne Galy,*,† and Jean-François Gerard†

Laboratory of Macromolecular Materials/IMP, UMR CNRS 5627, INSA Lyon, Bat. Jules Verne, 20 Avenue A. Einstein, 69621 Villeurbanne Cedex, France, and Guangzhou Institute of Geochemistry, Chinese Academy of Sciences, Wushan, Guangzhou 510640, China

Received: April 5, 2005; In Final Form: May 14, 2005

Molecular simulation techniques are used to find the basal spacing of organoclay on the basis of the energy minimum, using the canonical NVT ensemble. Then, the interlayer structure and mobility of alkyl chains are explored based on the interlayer atomic density profiles. Besides the basic lateral-monolayer arrangement, lateral-bilayer accompanied by partial a pseudo-trilayer and a transition structure between the two basic lateral models are observed. The later provides an excellent explanation about the reflection at 16 Å on XRD patterns in the literature. The atomic density profiles reveal that nitrogen atoms show stronger layering behavior than carbon atoms do. Our simulation demonstrates that the molecular mobility of the confined alkyl chains decreases from lateral-monolayer to lateral-bilayer with the increase of the intercalated surfactant. This is in accordance with the suggestion deduced from experiments. Furthermore, our simulation indicates that the mobility of the alkyl chains strongly depends on the surfactant arrangement rather than the surfactant packing density.

Introduction

Recently, organoclays, synthesized by modifying clay minerals with surfactants, have attracted great interest owing to their academic and industrial importance.[1−6] For example, organoclay-based nanocomposites exhibit remarkable improvement in properties when compared with virgin polymer or conventional micro- and macrocomposites. These improvements include increased strength and heat resistance, decreased gas permeability and flammability, and increased biodegradability of biodegradable polymer.[7] These improvements strongly depend on the structure and properties of the organoclays. Hence, understanding well the interlayer structure of organoclay and the interaction of surfactant−clay and surfactant−surfactant is essential for industrial applications and novel material design.

As we know, the most commonly used layer silicates (montmorillonite, hectorite, and saponite) in the preparation of polymer/layer silicate nanocomposites belong to the 2:1 type swelling clays (smectite). The thickness of a layer is ca. 0.97 nm. Because of isomorphic substitutions within the layers (for example, Al^{3+} replaced by Mg^{2+} or Fe^{2+}, or Mg^{2+} replaced by Li^+ in the octahedral sheet; Si^{4+} replaced by Al^{3+} in the tetrahedral sheet), the clay layer is negatively charged, which is counterbalanced by cations within the galleries. These cations are exchangeable and the sum of their charges is the cation exchange capacity (CEC). This CEC value determines the number of cationic surfactants that can be intercalated into the galleries by ion exchange. Clay minerals are hydrophilic and are only miscible with hydrophilic polymers. Hence, modifying the clay mineral surface with cationic surfactants, to convert the normally hydrophilic silicate surface to an organophilic surface, is a strategic step for the preparation of polymer/layer silicate nanocomposites.

Due to the fine particle, the low crystallizability, and the complicated chemical components of clays, detailed information about the interlayer structure and the atomic local environment in organoclay is rarely available from experimental measurements. So far, X-ray diffraction (XRD) is the most widely used technique to determine the structure of organoclays.[8−12] On the basis of the measured basal spacings and the length of the alkyl chains, various arrangement models have been proposed for the intercalated surfactants, including lateral-monolayer, lateral-bilayer, pseudo-trilayer, paraffin-monolayer, and paraffin-bilayer.[8] These idealized models are based on the assumption that the intercalated surfactants adopted all-trans conformation after intercalation. However, these idealized structural models were first shown to be unrealistic by Vaia et al.[13] on the basis of Fourier transform infrared spectroscopy (FTIR). They showed that alkyl chains can vary from liquidlike (disordered) to solidlike (ordered) and the confined amine chains exist in states with varying degrees of order in conformation. Furthermore, ^{13}C magic angle spinning nuclear magnetic resonance (^{13}C MAS NMR) demonstrates that there is an extensive coexistence of gauche and all-trans conformers from low to high packing density and the complete "solidlike" state does not exist.[14,15] Unfortunately, all these experimental results only provide an "average" state for the molecular arrangements and layering structure and it is difficult to quantify them.

More recently, molecular simulation has been proved to be a powerful technique to probe the detailed information about molecular arrangements and layering structure.[16−23] The simulated results provide not only the complementary evidence for the experimental results but also new insights for the microstructure of organoclay. For example, molecular simulation has demonstrated a mixed structure of paraffin-type and trilayer or quadrilayer in organoclay,[22] which has never been discussed in experimental studies. This reflects that the real structure of organoclay is more complicated than those proposed on the basis of the experimental measurements. With the application of

* Corresponding author. E-mail: hehp@gig.ac.cn; jocelyne.galy@insa-lyon.fr.

† Laboratory of Macromolecular Materials/IMP.

‡ Chinese Academy of Sciences.

10.1021/jp0517495 CCC: $30.25
Published on Web 06/17/2005

TABLE 1: The Charges of Atoms in Montmorillonite[a]

	Si	Al	Mg	Na	O_{bas}	O(H)	H	O_{api}
charge	1.2	3	2	1	−0.8	−1.7175	0.7175	−1.0

[a] Skipper et al., ref 25.

TABLE 2: Atom Charge for Hexadecyltrimethylammonium Cation ($HDTMA^+$)

	H	C (CH_2)	C (CH_3)[a]	C (CH_3)[b]	N
charge	0.053	−0.106	−0.159	0.248	−0.628

[a] $-CH_3$ at the end of amine chain. [b] $-CH_3$ binded with N.

molecular simulation in the study of organoclay, more and more detailed information on structure and physical-chemical characteristics will be provided. This is of great importance in the design and application of organoclay-based materials.

In this study, molecular simulation is used to find the basal spacing on the basis of the energy minimum and probe the layering behavior and interlayer structure of the constructed organoclays at an atomic scale. Comparison will be made between the simulated and experimental results mainly in terms of the basal spacings. On the basis of the atomic density profiles, the arrangement and the mobility of alkyl chains will be discussed and compared with the proposals deduced from experimental studies.

Methodology

The model construction was carried out with the Crystal Builder of Material Studio package on a PC computer. The first step in preparing the initial organoclay configuration for molecular simulation is to create a negatively charged montmorillonite framework. However, complete crystal structure information is not available because of the microcrystalline and poor ordering of smectite clays. Therefore, the atomic coordinates for montmorillonite in this study are based on the literature of Tsipursky and Drits.[24] The model unit cell parameters are $a = 5.18$ Å, $b = 8.98$ Å, $c = 12.8$ Å, $\alpha = \gamma = 90°$, and $\beta = 99°$ with a space group of $C2/m$.[24] In our idealized clay models, we assume that all layer charge comes from the substitution of aluminum by magnesium in the octahedral sheets.

Two basic types of montmorillonites (MMT-I and MMT-II) with different layer charges (−0.5 and −1 per unit cell, respectively) are built, with their unit cell formula given by $Na_x(Al_{4-x}Mg_x)Si_8O_{20}(OH)_4$. In the assumed unit cell formula, x is the layer charge and the unit cell is neutral.

The atomic charges in montmorillonite framework were directly taken from the literature provided by Skipper et al.[25] as shown in Table 1. These charge parameters proved to work well with the systems of hydrated clays and surfactant-modified clays.[22,23,25−28] Accordingly, there are two different unit cells built in this study. The unit cell formula for MMT-I is $Na_{0.5}(Al_{3.5}Mg_{0.5})Si_8O_{20}(OH)_4$ and that for MMT-II is $Na_1(Al_3Mg_1)Si_8O_{20}(OH)_4$.

Our periodic molecular simulation cell consists of 16 unit cells ($4a \times 4b \times 1c$), resulting in an overall size of $a = 20.72$ Å, $b = 35.92$ Å. The third dimension is built based on our assumption. Different conformations of hexadecyltrimethylammonium cation ($HDTMA^+$) were built using the Visualizer module of Materials Studio and the cations were minimized using the Amorphous Cell module and the Compass force field included in the Materials Studio package from Accelrys. The atom charge of $HDTMA^+$ is shown in Table 2. The construction of $HDTMA^+$/montmorillonite hybrid models was based on the assumption that all the interlayer cations in montmorillonite were replaced by $HDTMA^+$. Hence, two basic $HDTMA^+$/montmorillonite hybrid models were built, resulting from the corresponding unit cells with different layer charge. The two $HDTMA^+$/montmorillonite hybrid models were denoted as OM-I and OM-II, respectively. In OM-I, there were 8 $HDTMA^+$ cations residing in montmorillonite gallery while there were 16 $HDTMA^+$ cations in OM-II. The $HDTMA^+$ cations were manually placed into the montmorillonite interlayer with their longest chains oriented in a direction approximately parallel to the plane of the clay layers, similar to the method described in the literature.[22]

During the molecular simulations, the following basic strategies were taken:

1. The fractional coordinates of atoms in montmorillonite were fixed because of the assumption that the clay layer is rigid whereas the surfactant cations within the interlayer are freely movable.

2. The molecular simulation was carried out with the Compass force field and the Ewald summation method was used to calculate Coulombic interactions (COUL). A nonbond cutoff distance for the van der Waals interaction (VDW) was 8.5 Å.

In our present study, simulations were performed in the canonical NVT ensemble for 100 ps at 298 K with a time step of 0.001 ps, to let the system reach its equilibrium. This length of time proved to be sufficient for equilibration. On the basis of the plots of the energies to the basal spacings of $HDTMA^+$/montmorillonite hybrids, the basal spacing for the hybrid can be determined, which has the energy minimum. To save time, only the data (including coordinates, velocity, force, and statistic quantities) for the hybrid with the energy minimum are collected every 1 ps in the following 100 ps for further analysis.

Results and Discussion

Basal Spacings. To find the basal spacings of organoclays, a number of initial organoclay models were built with the same number of $HDTMA^+$ cations (8 cations in OM-I and 16 cations in OM-II), and different assumed d values and an interval of 1 Å. Then, let them reach equilibrium in the canonical NVT ensemble. Figure 1 shows the evolution of energy as a function of d for OM-I and OM-II. OM-I and OM-II reach an energy minimum when the d values are 14 and 19 Å, i.e., the basal spacings for OM-I and OM-II are 14 and 19 Å, respectively. This suggests that the basal spacing strongly depends on the mass of the intercalated alkyl chains.[8,12,22] In the following discussion, the above-mentioned organoclays with basal spacings of 14 and 19 Å are denoted as OM-I-14 and OM-II-19, respectively. Figure 2 displays snapshots of OM-I-14 and OM-II-19 after reaching equilibrium. In OM-I-14, the intercalated surfactants adopt a lateral-monolayer. However, in OM-II-19, most alkyl chains lie parallel to clay surface and result in a lateral-bilayer, whereas a minor amount of them adopt pseudo-trilayer, demonstrating the coexistence of lateral-bilayer and pseudo-trilayer. Our observation is in accordance with the proposal of the coexistence of lateral-bilayer and pseudo-trilayer, deduced from experimental XRD patterns.[29] This reflects that there is a transition from lateral-bilayer to pseudo-trilayer. During simulation, even if the surfactant chains are placed within the interlayer space randomly, the headgroups (nitrogen) of the alkyl chains will be close to the clay surface. This is due to the strong electrostatic interaction between the negative clay surface and the positive headgroups of the alkyl chains.

The plot of energy to d value for OM-I (Figure 1a) shows an asymmetric "W" shape with the two lower points at 14 and 16 Å, respectively. The energy of the $HDTMA^+$/montmorillonite

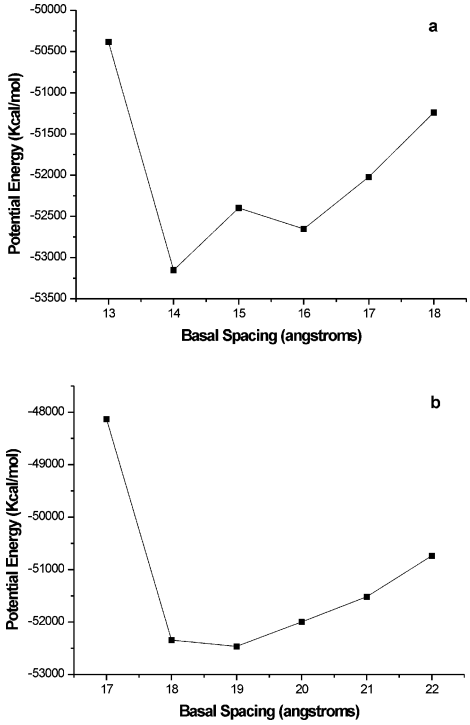

Figure 1. The evolution of energy as a function of *d* value for OM-I (a) and OM-II (b).

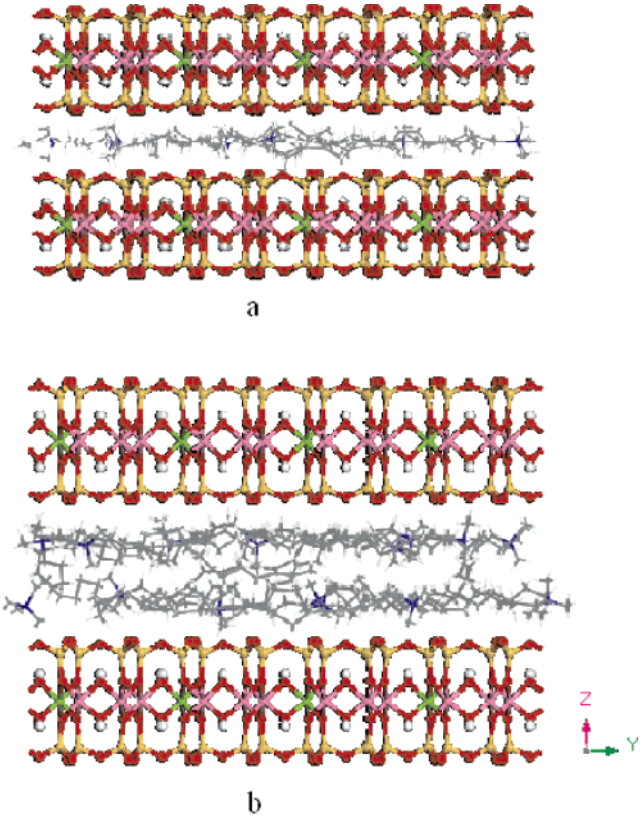

Figure 2. Snapshots of OM-I-14 (a) and OM-II-19 (b) after reaching equilibrium (100 ps).

hybrid with $d_{001} = 16$ Å is close to the minimum occurring at 14 Å and lower than the other neighboring points. To make sure, the simulations of organoclay with a *d* value at 14−17 Å were repeated several times with different initial configurations and similar results were gained, reflecting that our simulation results are credible. The asymmetric "W" shape of the plot of energy to the *d* value for OM-I suggests that the structure for

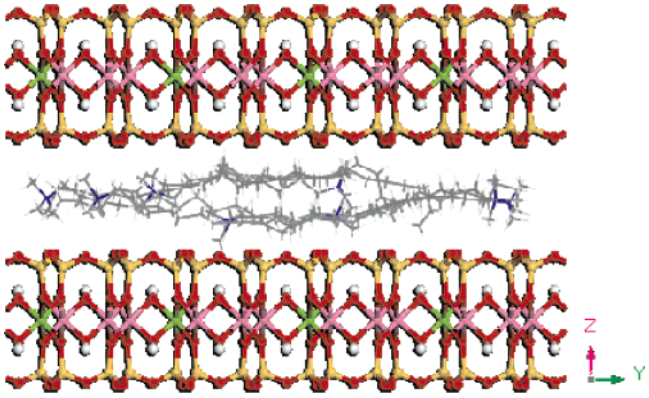

Figure 3. Snapshots of OM-I-16 after reaching equilibrium (100 ps).

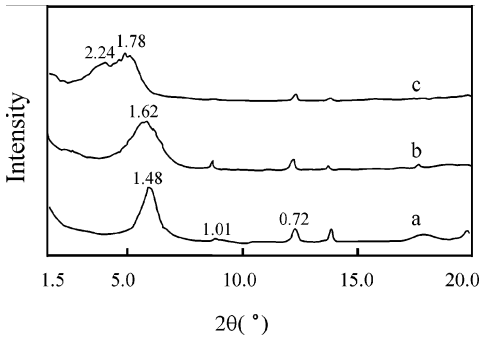

Figure 4. Experimental XRD patterns of HDTMA$^+$/montmorillonite with lateral-monolayer (a), lateral-bilayer (c), and the transition between the two arrangements (b).

the hybrid with $d_{001} = 16$ Å may be a metastable or a transition state, in which a partial overlapping between ends and/or end and headgroup among neighboring alkyl chains is observed (Figure 3). But there is no overlapping between two headgroups. This is due to the strong repulsive action between the headgroups with positive charges. In the literature, most previous studies displayed the basal spacing at 13−15 Å for the organoclay with lateral-monolayer and at 17.7−19.8 Å for those with lateral-bilayer.[8−12,30,31] However, the reflection at ca. 16 Å was really recorded in some previous experimental studies,[10,30,31] despite that it was not discussed in detail. In addition, our experiment about modifying montmorillonite with HDTMA$^+$ also showed a reflection at 16.2 Å when the arrangement of the intercalated surfactants transformed to lateral-bilayer (17.8 Å) from lateral-monolayer (14.8 Å) as shown in Figure 4. The consistence between the simulated and the experimental results strongly suggests that there is a transition structure between the lateral-monolayer and lateral-bilayer of the intercalated surfactants within the clay interlayer. Actually, the transition state between the transformations of different surfactant arrangements should exist extensively. For example, a pseudo-trilayer structure has been observed in both experimental and simulated results. In our opinion, it is a transition structure between lateral-bilayer and paraffin-monolayer. Furthermore, both our simulation for MO−II-19 and other reports[22,29] also demonstrate the existence of a mixed structure in organoclays. The existence of the mixed structure can well explain the broad reflections in the XRD patterns of organoclays. Possible schematics for the transformation from lateral-monolayer to lateral-bilayer are shown in Figure 5.

Interlayer Density Profiles. To establish the interlayer structure in the organoclays, the density distributions of various components in the systems in the direction normal to the clay surface are calculated. The density profiles for headgroups

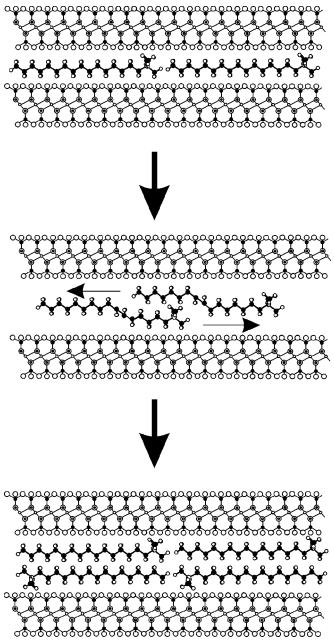

Figure 5. Possible schematics for the transformation from lateral-monolayer (top) to lateral-bilayer (bottom).

(nitrogen) and methyl and methylene groups (carbon) in OM-I with basal spacings of 14 and 16 Å (denoted as OM-I-16) and OM-II with basal spacing of 19 Å are shown in Figure 6.

The nitrogen atomic density profiles for OM-I-14 and OM-II-19 reveal strong layering behavior. All headgroups in OM-I-14 are distributed within one layer located in the middle of the interlayer while those in OM-II-19 are in two layers. The two well-separated and sharp peaks demonstrate a bilayer behavior. The nitrogen atomic density profile for OM-I-16 displays two closing peaks near the middle of the interlayer, which are different from that of the monolayer with a single peak and that of the bilayer with two well-separated peaks. The two closing peaks reflect that the interlayer structure for OM-I-16 is a transition state between monolayer and bilayer.

Similar to the nitrogen atomic density profiles, the carbon atomic density profiles (Figure 6) also demonstrate a similar layering behavior for the three abovementioned organoclay models. However, comparison between the nitrogen and carbon atomic density profiles for the same organoclay indicates that the distribution of nitrogen atoms has better layering behavior than carbon atoms do. This is due to the stronger electronic interaction between headgroups (positive charge) and the clay layer (negative charge). For alkyl chains, theoretical calculation[32] and experimental results[33] indicate that the most important factors governing their distribution are the nonbonded van der Waals interactions between the hydrogen atoms, which are weaker than the electronic interaction. This leads to the less ordered distribution of methyl and methylene groups than the headgroups, which is elucidated by the individual atomic density profiles. For nitrogen, the density distributions in the *z* direction are similar for all nitrogen atoms in the same layer whereas those for most carbon atoms are different from each other. As we know, the atomic density profile is a sum of the density profiles for all selected atoms in the organoclay. Accordingly, the distribution of nitrogen atoms has better layering behavior than that of carbon atoms.

Mobility of the Confined Alkyl Chains. The information on the molecular mobility of the intercalated surfactants was first obtained by Vaia et al.[13] using FTIR. Generally, as the interlayer packing density or the chain length decreases or the temperature increases, the intercalated chains adopt a liquidlike structure, i.e., the mobility of the chains increases. The following various experimental studies, including FTIR,[34−36] ^{13}C MAS NMR,[14,15,37] and Raman spectroscopy,[38] provided more detailed and/or complementary information about the mobility of the alkyl chains. Li and Ishida[34] proposed that the tails of alkyl chains have higher mobility than the headgroups when the alkyl chains radiate from the clay surface with increase of the packing density. This also has been found in other experimental studies of adsorption organics onto the surface and mesopores of various materials.[39−41] However, detailed information about the mobility of alkyl chains and individual atoms on alkyl chain is difficult to obtain by experiment.

To elucidate the mobility of the alkyl chains confined in organoclay as the lateral layer, the distribution ranges of individual carbon atoms in *x*, *y*, and *z* dimensions for OM-I-14, OM-I-16, and OM-II-19 were calculated. Our calculation shows that the distribution ranges of individual carbon atoms in *x*, *y*, and *z* dimensions in the same organoclay are identical whereas the unique difference among the different organoclays is the distribution in the *z* direction. Figure 7 shows the distribution ranges of individual carbon atoms in *x*, *y*, and *z* dimensions for the alkyl chain in OM-I-14, OM-I-16, and OM-II-19, which are calculated from the corresponding density profiles. From Figure 7, we can find that the distribution ranges of carbon atoms in OM-I-14 and OM-II-19 in *x* and *y* dimensions are similar whereas $\Delta dz_{\mathrm{OM-II-19}} < \Delta dz_{\mathrm{OM-I-14}}$ in the *z* direction. The variation of carbon atomic distribution in the *z* direction reflects that alkyl chains in OM-II-19 have lower mobility than those in OM-I-14. This reflects that the mobility of alkyl chains decreases with the increase of the surfactant within the clay interlayer and/or from lateral-monolayer to lateral-bilayer. The calculation of OM-I-16 indicates that $\Delta dz_{\mathrm{OM-I-16}} < \Delta dz_{\mathrm{OM-II-19}} < \Delta dz_{\mathrm{OM-I-14}}$ while the atomic distribution ranges in *x* and *y* dimensions are similar. Since the intercalated surfactant number in OM-I-14 and OM-I-16 is the same, our calculation demonstrates that the atomic mobility of the confined alkyl chains strongly depends on the chain arrangement.

To elucidate the possible effects from the interlayer distance, we constructed another model, OM-I-14-4, which has a *d* value of 14 Å and only has 4 $HDTMA^+$ cations within the montmorillonite interlayer. The atomic distribution range of model OM-I-14-4 was calculated and compared with that of OM-I-14. In both OM-I-14 and OM-I-14-4, a lateral-monolayer arrangement is adopted for the intercalated alkyl chains after reaching equilibrium. Our calculation demonstrates that the atomic distribution range for OM-I-14-4 in *x*, *y*, and *z* directions is identical with that for OM-I-14, despite the different number of surfactant cations within the interlayer. This further demonstrates that the surfactant arrangement is a key factor to control the distribution range of the atoms in the intercalated alkyl chains.

Our abovementioned discussion shows that, generally, the molecular mobility of the confined alkyl chains decreases from lateral-monolayer to lateral-bilayer with the increase of the intercalated surfactant cations. This is in accordance with the suggestion deduced from FTIR and NMR spectra.[13−15,34−37] The decrease of the alkyl chain mobility with the increase of the intercalated surfactant cations is due to the decreasing distance between the alkyl chains that increases the dipolar interactions.[37] However, in the case of the same basal spacing, the same lateral-monolayer arrangement, and different surfactant number, the mobility of the atoms in the alkyl chains is constant.

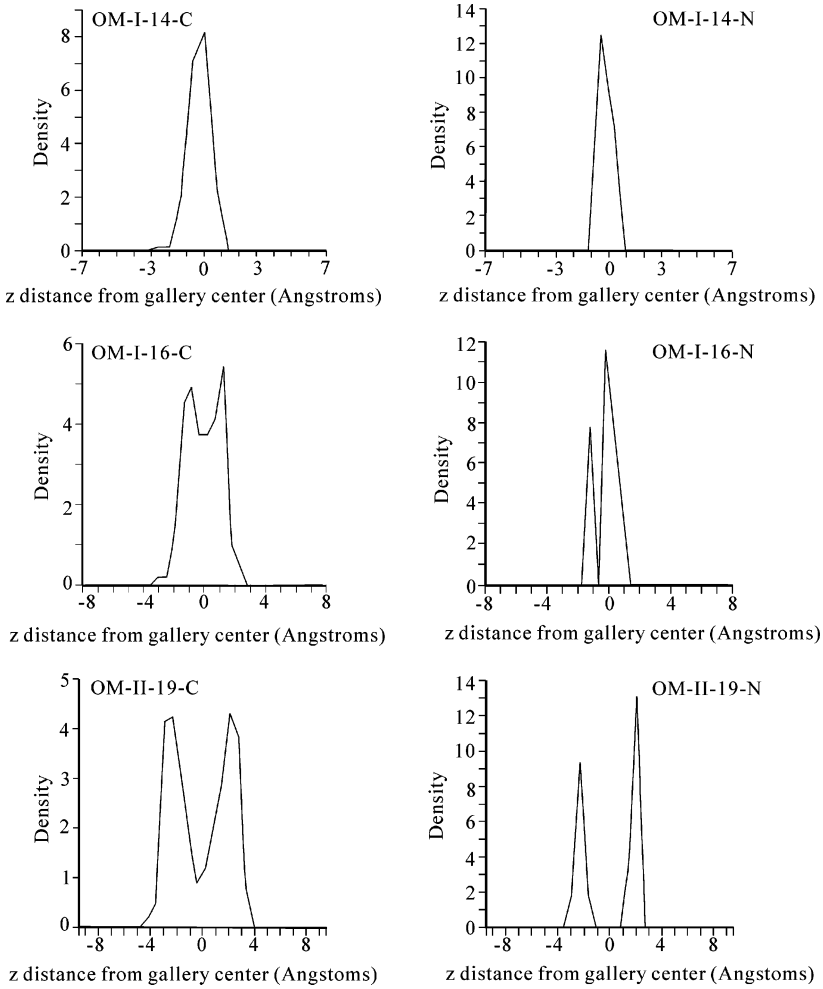

Figure 6. The density profiles for headgroups (nitrogen) (right) and methyl and methylene groups (carbon) (left) in OM-I-14, OM-I-16, and OM-II-19.

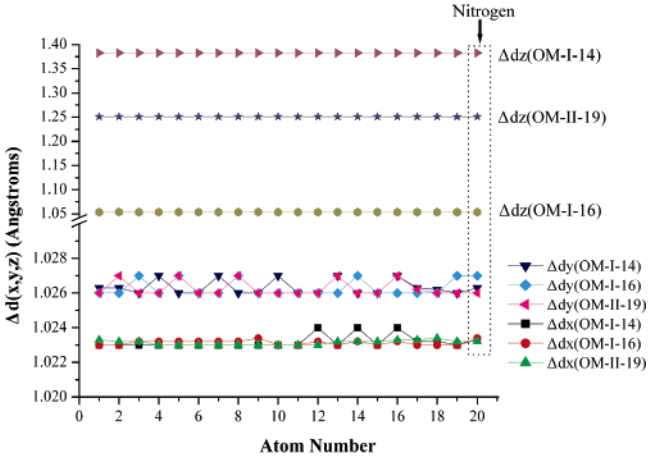

Figure 7. The distribution range of individual carbon atoms in *x*, *y*, and *z* dimensions for alkyl chain in OM-I-14, OM-I-16, and OM-II-19, respectively. (Atom numbers from 1 to 19 stands for carbon atoms from tail to headgroup and atom number 20 for the nitrogen atom.)

Conclusions

Our simulations elucidate that the interlayer structure of organoclay is more complicated than that deduced from experimental measurements. Besides a typical lateral-monolayer, a lateral-bilayer combining with partial pseudo-trilayer and a transition structure from lateral-monolayer to lateral-bilayer are observed in the present molecular simulations. In the transition structure from lateral-monolayer to lateral-bilayer, there is a partial overlapping between ends and/or end and headgroup among neighboring alkyl chains. This finding can well explain the reflection at 16 Å on XRD patterns in previous experimental measurements. Integration of the present and the previous simulations in the literature elucidates that the transformation between different surfactant arrangements is "gradual" rather than "stepwise". The nitrogen atomic density profile reveals stronger layering behavior than carbon atoms do. This results from the strong electronic interaction between the headgroups and the clay surface. Our simulation demonstrates that, generally, the molecular mobility of the confined alkyl chains decreases from lateral-monolayer to lateral-bilayer with the increase of surfactant within the clay interlayer. This is in accordance with the suggestion deduced from FTIR and NMR spectra. Further studies are underway to investigate the effects of charge origin and their distribution within octahedral and tetrahedral sheets on interlayer structure and molecular configuration, and the structure of the resultant polymer/clay nanocomposites.

Acknowledgment. The financial support of Fondation Franco-Chinoise pour la Science et ses Applications, Académie des Sciences, and Région Rhône-Alpes (France) is gratefully acknowledged. The authors are grateful to Dr. Zeng Qinghua for useful discussions and constructive suggestions. Prof. Sharon Hammes-Schiffer and the two anonymous reviewers are thanked for their constructive comments, suggestions, and helpful advice.

References and Notes

(1) Pinnavaia, T. J. *Science* **1983**, *220*, 365.
(2) Wu, J. H.; Lerner, M. M. *Chem. Mater.* **1993**, *5*, 835.
(3) Manias, E.; Hadziioannou, G.; Brinke, G. *Langmuir* **1996**, *12*, 4587.
(4) Wang, Z.; Pinnavaia, T. J. *Chem. Mater.* **1998**, *10*, 3769.
(5) Meier, L. P.; Nueesch, R.; Madsen, F. T. *J. Colloid Interface Sci.* **2001**, *238*, 24.
(6) Adebajo, M. O.; Frost, R. L.; Kloprogge, J. T.; Carmody, O. *J. Porous Mater.* **2003**, *10*, 159.
(7) Ray, S. S.; Okamoto, M. *Prog. Polym. Sci.* **2003**, *28*, 1539.
(8) Lagaly, G. *Clay Miner.* **1981**, *16*, 1.
(9) Tamura, K.; Nakazawa, H. *Clays Clay Miner.* **1996**, *44*, 501.
(10) Klapyta, Z.; Fujita, T.; Iyi, N. *Appl. Clay Sci.* **2001**, *19*, 5.
(11) Yui, T.; Yoshida, H.; Tachibana, H.; Tryk, D. A.; Inoue, H. *Langmuir* **2002**, *18*, 891.
(12) Zhu, J. X.; He, H. P.; Guo, J. G.; Yang, D.; Xie, X. D. *Chin. Sci. Bull.* **2003**, *48*, 368.
(13) Vaia, R. A.; Teukolsky, R. K.; Giannelis, E. P. *Chem. Mater.* **1994**, *6*, 1017.
(14) Wang, L. Q.; Liu, J.; Exarhos, G. J.; Flanigan K. Y.; Bordia R. *J. Phys. Chem. B* **2000**, *104*, 2810.
(15) He, H. P.; Frost, R. L.; Deng, F.; Zhu, J. X.; Weng, X. Y.; Yuan, P. *Clays Clay Miner.* **2004**, *52*, 350.
(16) Teppen, B.; Rasmussen, K.; Bertsch, P. M.; Miller, D. M.; Schafer, L. *J. Phys. Chem. B* **1997**, *101*, 1579.
(17) Hackett, E.; Manias, E.; Giannelis, E. P. *J. Chem. Phys.* **1998**, *108*, 7410.
(18) Janeba, D.; Čapková, P.; Weiss, Z. *J. Mol. Model.* **1998**, *5*, 8.
(19) Pospíšil, M.; Čapková, P.; Weiss, Z.; Maláč, Z.; Šimoník, J. *J. Colloid Interface Sci.* **2002**, *245*, 126.
(20) Čapková, P.; Burda, J. V.; Weiss, Z.; Schenk, H. *J. Mol. Model.* **1999**, *5*, 8.
(21) Heinz, L.; Castelijns, H. J.; Suter, U. W. *J. Am. Chem. Soc.* **2003**, *125*, 9500.
(22) Zeng, Q. H.; Yu, A. B.; Lu, G. Q.; Standish, R. K. *Chem. Mater.* **2003**, *15*, 4732.
(23) Zeng, Q. H.; Yu, A. B.; Lu, G. Q.; Standish, R. K. *J. Phys. Chem. B* **2004**, *108*, 10025.
(24) Tsipursky, S. I.; Drits, V. A. *Clay Miner.* **1984**, *19*, 177.
(25) Skipper, N. T.; Refson, K.; McConnell, J. D. C. *Clays Clay Miner.* **1995**, *43*, 249.
(26) Boek, E. S.; Coveney, P. V.; Skipper, N. T. *J. Am. Chem. Soc.* **1995**, *117*, 12608.
(27) Smith, D. E. *Langmuir* **1998**, *14*, 5959.
(28) Greathouse, J. A.; Refson, K.; Sposito, G. *J. Am. Chem. Soc.* **2000**, *122*, 11459.
(29) Xi, Y. F.; Ding, Z.; He, H. P.; Frost, R. L. *J. Colloid Interface Sci.* **2004**, *277*, 116.
(30) Favre, H.; Lagaly, G. *Clay Miner.* **1991**, *26*, 19.
(31) Li, Y. Q.; Ishida, H. *Chem. Mater.* **2002**, *14*, 1398.
(32) Tasi, G.; Mizukami, F. *J. Math. Chem.* **1999**, *25*, 55.
(33) Okamura, E.; Umemura, J.; Takenaka, T. *BBA-Biomembr.* **1985**, *812* (1), 139.
(34) Li, Y. Q.; Ishida, H. *Langmuir* **2003**, *19*, 2479.
(35) He, H. P.; Frost, L. R.; Zhu, J. X. *Spectrochim. Acta A* **2004**, *60*, 2853.
(36) Xi, Y. F.; Ding, Z.; He, H. P.; Frost, R. L. *Spectrochim. Acta A* **2005**, *61*, 515.
(37) Khatib, K.; Francois, M.; Tekely, P.; Michot, L. J.; Bottero, J. Y.; Baudin, I. *J. Colloid Interface Sci.* **1996**, *183*, 148.
(38) He, H. P.; Frost, L. R.; Xi, Y. F.; Zhu, J. X. *J. Raman Spectrosc.* **2004**, *35*, 316.
(39) Badia, A.; Gao, W.; Singh, S.; Demers, L.; Cuccia, L.; Reven, L. *Langmuir* **1996**, *12*, 1262.
(40) Gao, W.; Dickinson, L.; Grozinger C.; Morin, F. G.; Reven, L. *Langmuir* **1996**, *12*, 6429.
(41) Simonutti, R.; Comotti, A.; Bracco, S.; Sozzani, P. *Chem. Mater.* **2001**, *13*, 771.